

# Depth to Anatomy: Learning Internal Organ Locations from Surface Depth Images

Eytan Kats <sup>1</sup>, Kai Geissler <sup>2</sup>, Jochen G. Hirsch <sup>2</sup>, Daniel Mensing <sup>2</sup>, Stefan Heldman <sup>2</sup>, Mattias P. Heinrich <sup>1</sup>

<sup>1</sup> Institute of Medical Informatics, University of Luebeck, Luebeck, Germany

<sup>2</sup> Fraunhofer Institute for Digital Medicine MEVIS, Bremen, Germany

## Abstract

Automated patient positioning plays an important role in optimizing scanning procedure and improving patient throughput. Leveraging depth information captured by RGB-D cameras presents a promising approach for estimating internal organ positions, thereby enabling more accurate and efficient positioning. In this work, we propose a learning-based framework that directly predicts the 3D locations and shapes of multiple internal organs from single 2D depth images of the body surface. Utilizing a large-scale dataset of full-body MRI scans, we synthesize depth images paired with corresponding anatomical segmentations to train a unified convolutional neural network architecture. Our method accurately localizes a diverse set of anatomical structures, including bones and soft tissues, without requiring explicit surface reconstruction. Experimental results demonstrate the potential of integrating depth sensors into radiology workflows to streamline scanning procedures and enhance patient experience through automated patient positioning. The implementation and pretrained models are publicly available at <https://github.com/EytanKats/orgloc>.

## Keywords

Radiology workflow, Organs localization

## Article informations

Corresponding author: [eytan.kats@uni-luebeck.de](mailto:eytan.kats@uni-luebeck.de)

©YYYY Kats and Heinrich. License: CC-BY 4.0

## 1. Introduction

The growing demand for radiology examinations underscores the need to optimize scanning procedures to reduce patient wait times and improve operational efficiency. A critical, yet time-intensive, aspect of this process is the patient preparation and planning phase, which is essential for optimizing image quality and diagnostic accuracy (Van Rooyen and Pitcher, 2020). This phase typically involves manual positioning of the patient followed by scout imaging to facilitate detailed geometric planning for subsequent diagnostic scans. In standard clinical practice, a radiologic technologist initially aligns the patient on the table, often relying on external anatomical landmarks or laser positioning guides to approximate the region of interest. Once the patient is positioned inside the bore, a set of low-resolution, multi-planar scout images is acquired. These images are then used to visually confirm the patient's position and to manually plan the geometry of the diagnostic sequences, such as slice orientation, field-of-view, and scan range (Koken et al., 2009).

Despite recent advances in radiology hardware and software, the automation of patient positioning remains a largely underexplored area compared to other aspects of scan accel-

eration or reconstruction (Shafieizargar et al., 2023; Heckel et al., 2024). Traditional workflows still rely heavily on the experience and judgment of technologists. This manual planning process is both operator-dependent and time-consuming, particularly in complex examinations involving multiple regions or when precise anatomical targeting is required. Furthermore, variability in technologist expertise and patient anatomy can lead to inconsistent positioning, necessitating repeat localizers or even additional diagnostic scans, thereby increasing overall examination time and reducing scanner throughput (Danilouchkine et al., 2005).

Automated patient positioning systems, capable of accurately identifying and localizing the anatomical region of interest, hold considerable promise for streamlining radiology workflows by automatically adjusting the patient table to the optimal position. By reducing reliance on manual table adjustments and anatomical landmark estimation, these systems can minimize inter-operator variability, decrease setup time, and mitigate the risk of positioning errors, improving both imaging efficiency and diagnostic consistency across radiology departments.

Among the emerging technological approaches in this area, RGB-D camera-based systems have shown notable potential in enhancing patient setup and positioning (Booij

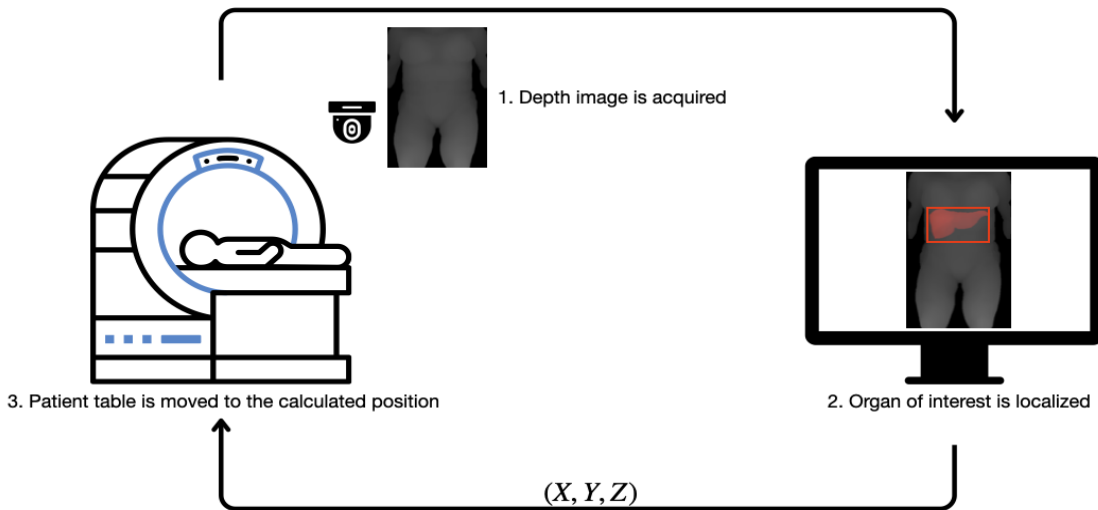


Figure 1: Overview of the proposed automated patient positioning workflow. A depth sensor installed above the scanner bore captures a depth image of the patient lying on the table. This image is processed by a trained model that predicts the 3D bounding box of the target organ. The scanner table is then automatically adjusted to align the organ of interest with the center of the imaging field-of-view, reducing the need for manual repositioning and scout scans.

et al., 2021, 2019). These integrated systems use depth-sensing to generate surface maps of the patient’s body. By analyzing these surface contours, it becomes possible to detect and localize key anatomical landmarks, which serve as proxies for internal anatomical regions of interest. This information can then be used to infer the optimal imaging volume and adjust the patient table position automatically prior to scan acquisition, without the need for scout imaging. For example, İncetan et al. (2020) demonstrated the utility of RGB-D sensors in automatically localizing target regions such as the head and thorax with high spatial accuracy. Similarly, Karanam et al. (2020) employed depth-aware landmark detection models to support robust, contactless patient positioning in MRI and CT workflows.

In the proposed workflow, a depth sensor is integrated into the room above the scanner bore to capture a depth image of the patient lying on the table. This depth image is then processed by the trained model, which outputs the 3D coordinates of the bounding box enclosing the organ of interest. Based on this prediction, the scanner table can be automatically adjusted to ensure that the relevant anatomy is optimally centered within the imaging field-of-view, minimizing the need for manual repositioning or iterative scout imaging (Figure 1). This approach offers a contactless, fast, and standardized method of patient localization, which could be particularly beneficial in high-throughput clinical environments or for procedures requiring precise anatomical targeting.

To ensure robust performance across a wide range of anatomical variations and body types, we train our model

on a large-scale dataset consisting of approximately 10,000 whole-body MRI scans from the German National Cohort (NAKO) study (Bamberg, 2022). This dataset includes subjects of diverse ages, body sizes, and physiological characteristics, enabling the model to generalize effectively across different patient populations. Our experimental evaluation demonstrates the effectiveness of the proposed method in accurately localizing 41 distinct internal anatomical structures, including bones and soft tissue organs, using only depth images.

The key contributions of this work are as follows:

1. We demonstrate the feasibility and effectiveness of a learning-based framework for estimating 3D locations of internal anatomical structures solely from depth images of the patient’s body surface.
2. We introduce a convolutional neural network architecture, Pixel-to-Voxel (Pix2Vox), which maps 2D depth images to 3D volumetric segmentation masks, enabling organ localization from a single surface view.
3. We validate the generalizability of our model across a wide range of body types and anatomical variations by training and evaluating on a large-scale, population-level dataset comprising approximately 10,000 whole-body MRI scans.

## 2. Related Works

The prediction of internal anatomical structures from external body surface representations has gained increasing attention due to its potential to enable non-invasive, ef-

ficient, and patient-specific modeling. Early work by Wu et al. (2018) introduced a learning-based framework that generates volumetric anatomical phantoms of skeletal and pulmonary structures from triangulated meshes of the patient’s external surface. This study demonstrated the feasibility of inferring detailed 3D internal anatomy from external geometry using deep models trained on co-registered body surface and internal organ data.

### Intermediate 3D representations for internal anatomy estimation.

Several approaches address the prediction of internal anatomy by first deriving an intermediate 3D representation from depth images, which is then used to infer internal structures. Building on the integration of statistical human body models with internal anatomy, recent research has extended the widely adopted Skinned Multi-Person Linear (SMPL) model (Loper et al., 2015) to incorporate internal organ representations. The original SMPL is a parametric, skinned 3D body model that encodes human pose and shape with a low-dimensional set of learned parameters, enabling the synthesis of realistic body meshes through linear blend skinning. Guo et al. (Guo et al., 2022) proposed SMPL-A, which augments SMPL with deformable internal organ geometries, allowing organ shapes to adapt dynamically with body pose. While effective in modeling pose-aware internal anatomy, SMPL-A requires a patient-specific full-body mesh to initialize internal organ shapes, limiting its generalizability and real-time applicability in clinical environments. Similarly, OSSO (Keller et al., 2022) and BOSS (Shetty et al., 2023) infer internal organ shapes and locations by optimizing anatomical plausibility within the SMPL framework based on external body surface meshes. Extending this paradigm, the HIT (Human Internal implicit Tissues) framework (Keller et al., 2024) employs a deep implicit function to predict continuous volumetric tissue distributions conditioned on a parametric body surface mesh. HIT leverages large-scale synthetic datasets and a canonical space aligned with SMPL to infer anatomically coherent internal structures. Despite promising results, these SMPL-based approaches depend on accurate surface mesh reconstruction and template fitting, which are computationally intensive. The LOOC framework (Henrich and Mathis-Ullrich, 2025) introduces an implicit volumetric model to infer internal organ locations and approximate shapes from depth-derived surface point clouds.

**Prediction of 2D organ projections.** Recent studies by Geißler et al. (2025) and Kats et al. (2025) successfully utilize convolutional neural networks (CNNs) that operate directly on depth maps to predict 2D projections of organs in the coronal plane. These works demonstrate that CNNs can effectively extract spatial cues from external body surfaces to infer accurate organ locations.

**Prediction of 3D features from 2D depth images.** Teixeira et al. (Teixeira et al., 2023) proposed a CNN-based method that directly estimates critical scan planning parameters—such as lung centroids and patient isocenter—from raw depth images. This approach bypasses SMPL-based registration and operates solely on depth data, providing a lightweight and robust solution for specific imaging tasks such as isocenter calculation in thoracic MRI.

In contrast to previous work on organ localization, our method introduces a lightweight, end-to-end framework that directly predicts explicit 3D bounding boxes and estimates shapes for 41 internal anatomical structures from a single depth image. Leveraging a unified Pix2Vox convolutional architecture, our approach eliminates the need for intermediate steps such as 3D surface reconstruction or canonical space registration, enabling rapid inference and practical integration into clinical workflows. To foster reproducibility and facilitate further research, our code and pretrained models are publicly available at <https://github.com/EytanKats/orgloc>.

## 3. Materials and Methods

In this study, we leverage 10,020 full-body MRI scans from the National Cohort Study of Germany (NAKO) dataset (Bamberg, 2022). This large and diverse dataset enables us to capture a broad spectrum of anatomical variability across age, sex, and body habitus, providing a robust foundation for training generalizable models of internal anatomy. Since paired depth images and organ segmentations are not natively available in the dataset, we synthetically generate training pairs from the MRI data.

To create depth images, we simulate depth sensor output by rendering the outer contours of the patient’s body from MRI volumes, mimicking the top-down perspective of real-world RGB-D sensors typically mounted above the scanner table. Simultaneously, we apply state-of-the-art automated segmentation tools to extract ground-truth 3D labels for 41 internal anatomical structures, including bones and soft tissue organs (Section 3.1).

The resulting dataset, composed of 2D depth images paired with corresponding 3D anatomical segmentations, serves as the training input for our proposed learning pipeline. We devised CNN and train Pix2Vox convolutional neural network, which maps each 2D depth image to a 3D volumetric prediction of the target organ bounding boxes (Section 3.2).

### 3.1 Data Preparation

To simulate depth images from MRI volumes, we begin by normalizing each 3D MRI scan to the intensity range  $[0, 1]$ . Next, we apply a global intensity threshold of 0.02 to generate a binary mask that captures the patient’s body.

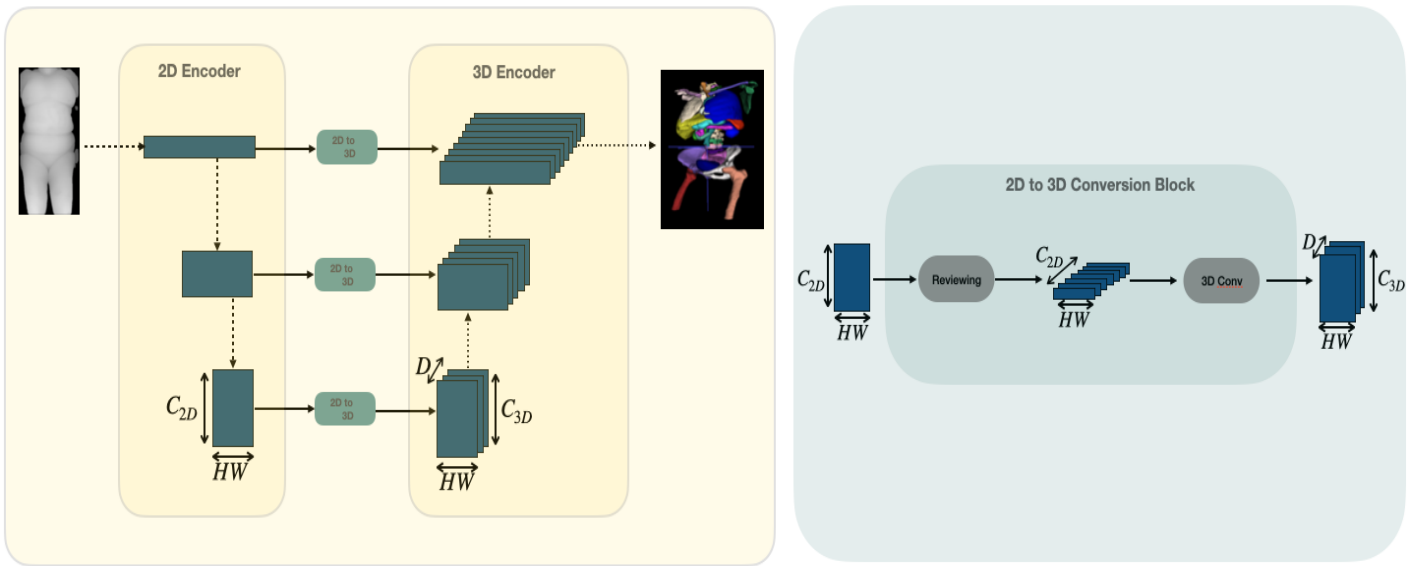


Figure 2: Overview of the proposed hybrid Pix2Vox network architecture. Left: The full model consists of a 2D encoder, 3D decoder, and custom 2D-to-3D conversion layers that connect the encoder and decoder at the bottleneck and each skip connection. Right: A detailed view of the 2D-to-3D conversion block. This module reshapes the 2D feature maps by unsqueezing a feature dimension and applying a 3D convolution to produce a volumetric representation suitable for further 3D processing. For clarity, the batch dimension is omitted from all illustrated tensor shapes.

Small noise components and isolated artifacts are subsequently removed using binary morphological opening with a spherical structuring element, producing a cleaner mask. We then extract 2D orthographic depth projections in the coronal plane, simulating the top-down view of a depth sensor positioned above the patient. Specifically, for each pixel in the image plane, the depth value is computed as the closest point of intersection along the anterior-posterior axis with the segmented patient's body. The resulting depth maps are normalized again to the range  $[0, 1]$ . To suppress non-anatomical structures such as the patient table and background noise, we apply a depth cutoff, setting all pixel values below 0.3 to 0. This effectively removes table artifacts and regions far below the simulated camera plane. Finally, to refine the depth image, we apply grayscale morphological opening, which smooths remaining artifacts while preserving significant anatomical features such as limb contours and body curvature. The resulting depth images offer a standardized approximation of the patient's body surface from a fixed sensor viewpoint and serve as input to our learning framework.

To generate high-quality anatomical reference labels, we leveraged recent state-of-the-art automated whole-body MRI segmentation tools, including TotalSegmentatorMRI (D'Antonoli et al., 2024), MRSegmentator (Häntze et al., 2024), and TotalVibeSegmentator (Graf et al., 2024). These models, trained on large-scale MRI datasets, are capable of accurately segmenting a wide range of anatomical structures with high spatial precision. To further increase the number

of segmented labels, the MR volumes were converted into synthetic CT volumes to utilize segmentation models available for CT data (Wasserthal et al., 2023; Jaus et al., 2023), following the approach described in Mensing et al. (2025). An aggregation procedure was implemented to select, for each anatomical structure, the segmentation mask with the highest accuracy. When a structure was available from multiple models, MR-based segmentations were prioritized over CT-based ones. The MRI segmentation models were ranked according to the similarity of their training data to our dataset, in the following order: TotalVibeSegmentator, MRSegmentator, and TotalSegmentatorMRI. For structures exclusively available from CT-based models, TotalSegmentator was preferred over Atlas DAP. The resulting aggregated masks encompass 137 distinct structures, including organs, vessels, bones, and tissue types.

Given the varying quality of automated segmentations across different structures and the need for relevance to clinical workflow optimization, we performed a careful selection process. In consultation with domain experts, and through extensive visual inspection of the output masks, we selected 41 anatomical structures (Table 1). These included bones and soft-tissue organs that are both (1) of practical importance for guiding scan planning and patient positioning, and (2) reliably segmented across a broad range of patients. To further improve the consistency of the labels and reduce artifacts introduced by the segmentation models, we applied a series of post-processing steps. These included hole filling to restore anatomical completeness,

and connected components analysis to eliminate spurious isolated regions or misclassified voxels. These refinements ensured cleaner and more robust ground-truth volumes for training the model.

Table 1: Selected organ labels grouped by tissue type

Soft Tissue Organs	Bones	
spleen	scapula left	vertebrae_T12
kidney right	scapula right	vertebrae_T11
kidney left	clavicula left	vertebrae_T10
liver	clavicula right	vertebrae_T9
stomach	femur left	vertebrae_T8
pancreas	femur right	vertebrae_T7
lung right	hip left	vertebrae_T6
lung left	hip right	vertebrae_T5
trachea	sacrum	vertebrae_T4
thyroid gland	vertebrae L5	vertebrae_T3
duodenum	vertebrae L4	vertebrae_T2
urinary bladder	vertebrae L3	vertebrae_T1
aorta	vertebrae L2	
heart	vertebrae L1	

### 3.2 Pix2Vox Model

For training, we employ a U-shaped convolutional neural network architecture that takes as input 2D depth images representing the patient’s body surface and outputs 3D volumetric segmentation masks of internal anatomical structures (Figure 2). The network is designed to bridge the dimensional gap between 2D input and 3D output using a combination of standard 2D encoder and 3D decoder modules, connected via custom 2D-to-3D conversion layers placed at the bottleneck and each skip connection.

The encoder consists of a series of convolutional and pooling layers that extract increasingly abstract spatial features from the input depth image. These features are encoded as 2D feature maps of shape  $b \times c \times h \times w$ , where  $b$  denotes the batch size,  $c$  the number of channels, and  $h$ ,  $w$  the spatial height and width, respectively.

To transition from 2D to 3D, we introduce conversion layers that reshape and transform the encoded 2D features into a format suitable for the 3D decoder. Specifically, for a given layer  $l$ , we apply the following transformation:

1. First, we unsqueeze the 2D feature maps along a new feature axis, producing a 5D tensor of shape  $b \times 1 \times c \times h \times w$ . This tensor is interpreted as a volumetric feature map with a singleton depth dimension and channel depth equal to  $c$ .
2. Next, we apply a 3D convolutional layer with kernel size  $k_l \times 1 \times 1$ , stride  $s_l \times 1 \times 1$ , and output feature size  $f_l$ .

The  $k_l$ ,  $s_l$ , and  $f_l$  parameters are chosen individually for each layer  $l$  to produce an appropriate depth dimension and number of features for input into the 3D decoder (Figure 2).

The decoder is composed of standard 3D convolutional layers with upsampling operations to progressively reconstruct the full volumetric segmentation output. The decoder also incorporates skip connections from the encoder, each of which passes through its corresponding 2D-to-3D conversion layer to ensure dimensional compatibility.

This hybrid 2D-3D design enables efficient processing of the 2D input depth images while producing dense 3D predictions, balancing memory efficiency with spatial expressiveness.

## 4. Experiments and Results

To train our model, we randomly selected 8,528 pairs of depth images and their corresponding segmentation masks from the preprocessed dataset (Section 3.1). A separate validation set of 494 samples was used to monitor training performance and guide model selection and hyperparameter tuning. For evaluation, we employed a dedicated test set of 998 samples, which was held out during training. This large and diverse set of examples enables a thorough assessment of the model’s performance and provides strong evidence of its ability to learn robust and generalizable features across range of anatomical variations.

### 4.1 Training and evaluation details

We train our model in a multi-label segmentation setting, applying a sigmoid activation function at the final layer to independently predict the presence of each anatomical structure. The loss function is a weighted sum of Dice loss and binary cross-entropy loss, with both components equally weighted at 0.5. To enhance the model’s robustness to anatomical variability and patient positioning, we apply data augmentations including random shifts, scaling, and rotations during training. This encourages the model to generalize across a broader range of spatial configurations. Training is performed using the Adam optimizer with an initial learning rate of 0.001. We apply a linear warm-up strategy over the first 1,000 training steps to stabilize early training, followed by cosine annealing to gradually reduce the learning rate to zero over the remaining steps. We use a batch size of 8, and training is carried out for 15,000 steps in total. To further improve robustness and reduce prediction noise during evaluation, we apply a post-processing step based on connected component analysis. This removes small, isolated predictions that are spatially distant from the main predicted regions, thereby reducing the likelihood of large errors caused by spurious or misclassified voxels.

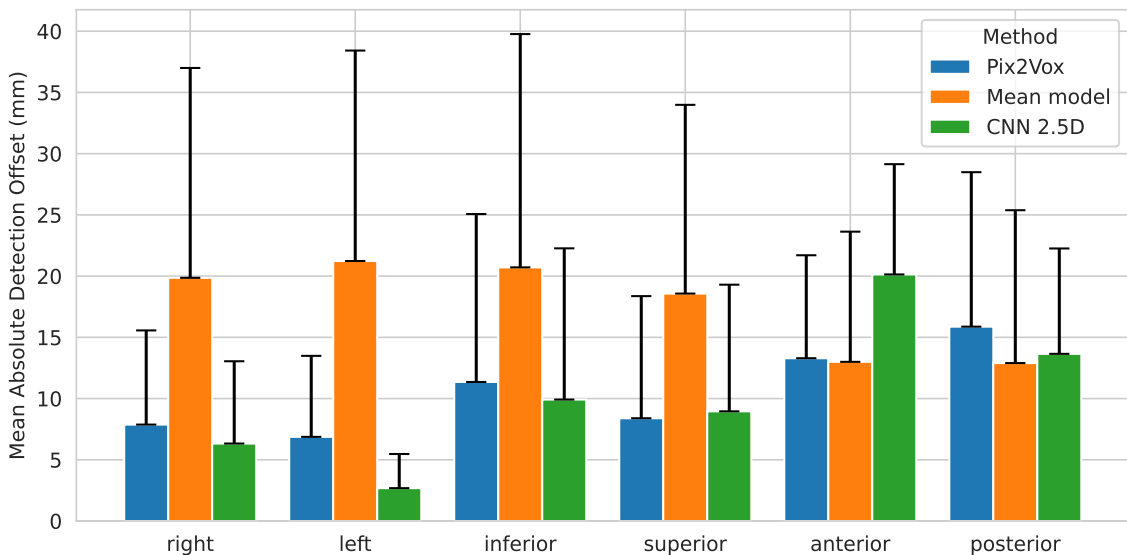


Figure 3: Mean absolute Detection Offset Error (DOE) averaged across all organs for each bounding box side (left-right, anterior-posterior, superior-inferior). The CNN models demonstrates strong localization accuracy, particularly in the coronal (left-right) and vertical (superior-inferior) dimensions, significantly outperforming the mean model baseline. They achieve sub-10mm average error in the coronal plane. Performance degrades along the anterior-posterior axis due to limited depth cues available from the coronal input image. Standard deviation is depicted as error bars extending in the positive direction only.

#### 4.2 Baselines

**Mean model.** Given the well-aligned patient positioning in the NAKO MRI dataset and the consistent anatomical layout across subjects, we exploit this property to construct a mean segmentation baseline model. Despite variability in patient-specific characteristics such as age, height, and body shape, the high degree of spatial alignment in the dataset enables the generation of an average anatomical representation from the training data. To build this baseline, we aggregate all ground truth segmentations from the training set by computing the voxel-wise mean across all examples. Specifically, each label channel is summed across all training subjects, divided by the total number of samples, and then thresholded at 50% of the maximum voxel intensity for that label to obtain a binary segmentation. This process yields a static, patient-agnostic model that serves as a reference for evaluating the effectiveness of learning-based methods. Although simplistic, this mean model provides a strong benchmark in settings with highly standardized acquisition protocols, offering insights into how much a learning-based model improves upon pure spatial prior knowledge.

**2.5D CNN.** Inspired by prior work by Geißler et al. (2025) and Kats et al. (2025), which leverage 2D CNNs to predict coronal plane projections of anatomical structures, we extend this concept to a more comprehensive 2.5D setting. Specifically, we employ separate 2D CNN models to predict the organ projections onto all three principal anatomical

planes: coronal, sagittal, and axial. Each model is trained independently to generate a binary mask representing the projection of target anatomical structures in its respective plane, using the same depth image as input. By aggregating the outputs of these three models, we can infer 3D bounding boxes for each organ by combining the spatial extents across all dimensions. This approach offers a computationally efficient alternative to full 3D segmentation, while still capturing spatial context through multi-planar analysis.

#### 4.3 Metrics

We evaluate the localization and segmentation performance of all models using a combination of complementary metrics that capture both spatial accuracy and anatomical shape fidelity. Bounding boxes are derived from the volumetric segmentation masks produced by the mean model, the Pix2Vox model, and the three-plane predictions of the 2.5D CNN. To quantify localization accuracy, we calculate the Mean Absolute Detection Offset Error (DOE), defined as the absolute distance between the corresponding faces of the predicted and ground truth bounding boxes along each axis. To better understand model behavior in different spatial dimensions, DOE is reported separately for each side of the bounding box (e.g., left, right, anterior, posterior, superior, inferior). This directional breakdown allows us to assess how accurately each method positions the anatomical structures along the full 3D extent. Importantly, this metric

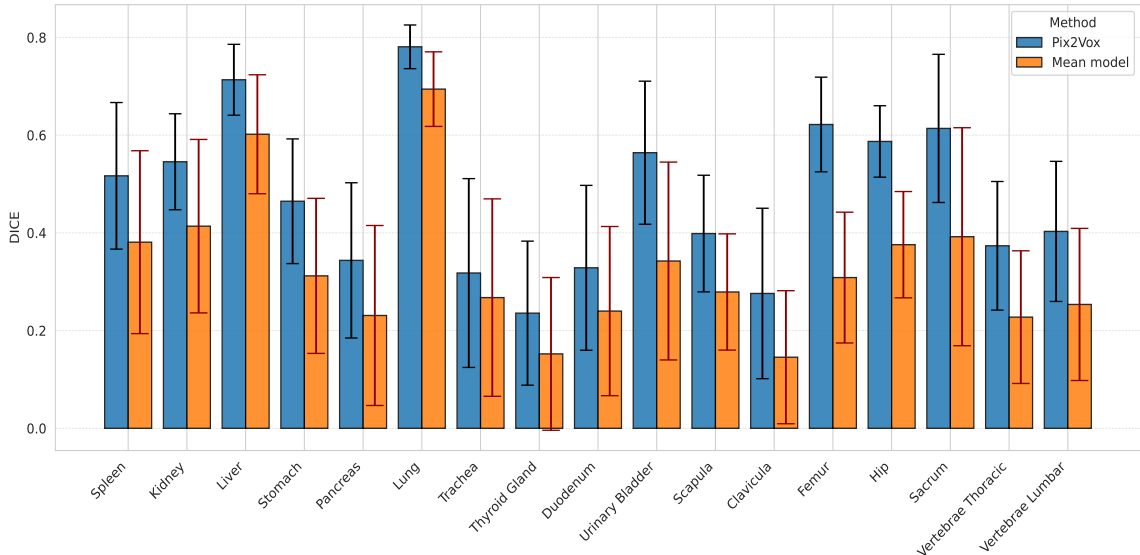


Figure 4: Dice coefficient for volumetric organs segmentation. Values are averaged for bilateral organs (e.g., kidneys, lungs) and vertebral subgroups (thoracic and lumbar vertebrae). Pix2Vox significantly outperforms the baseline, demonstrating its ability to generate accurate, patient-specific organ segmentations from a single coronal depth image.

reflects practical constraints in clinical imaging scenarios, particularly in automated patient positioning and scan planning, where under- or over-estimating organ boundaries can lead to suboptimal coverage or increased scan time. To assess the model’s ability to reconstruct organ shape, we compute the Average Symmetric Surface Distance (ASSD) between the predicted and ground truth segmentations, which captures discrepancies at the organ boundary. In addition, we report the Dice coefficient as a standard volumetric overlap metric. Both Dice and ASSD are calculated only for models that produce full 3D volumetric predictions, enabling us to evaluate how well the organ shape can be recovered from 2D depth image inputs alone.

#### 4.4 Results

Quantitative analysis using the Detection Offset Error (DOE) highlights the strong performance of the proposed Pix2Vox model in localizing internal organs in 3D space based solely on a single coronal depth image (Figure 3). Specifically, in the coronal plane, Pix2Vox demonstrates a more than twofold improvement in mean absolute DOE compared to the mean model baseline, achieving an average localization error of less than 10mm across all evaluated organs. However, performance degrades when localizing organs along the anterior-posterior (depth) axis, where the model shows higher variance and larger prediction errors. This limitation is not unexpected, given that the coronal depth image inherently provides less depth-specific information. Nonetheless, the ability of the CNN to infer organ depth from contextual and structural cues in a single 2D image remains noteworthy, demonstrating the model’s strong capacity for generaliza-

tion. The 2.5D CNN approach, which integrates predictions from coronal, sagittal, and axial projections, exhibits superior localization performance in the coronal plane and achieves more robust bounding box estimation in lateral and vertical dimensions. However, it still underperforms in predicting organ position along the depth axis. This shortfall may be attributed to the limited representational capacity of the 2D projection-based architecture and the absence of a fully 3D decoding mechanism, which constrains the model’s ability to jointly reason across spatial dimensions.

Quantitative evaluation using the Dice coefficient and ASSD)(Figure 4 and Figure 5), alongside qualitative visualizations of Pix2Vox predictions (Figure 6), reveals the model’s remarkable ability to infer internal organ shape from a single 2D depth image. Unlike the mean model baseline, which simply reflects anatomical averages, Pix2Vox demonstrates a substantial improvement in both overlap and surface accuracy metrics. This performance gap highlights the model’s capacity to move beyond population-level anatomical assumptions and instead learn spatially-aware, patient-specific volumetric representations directly from depth cues present in surface imagery. The model’s strong performance across diverse organ types, sizes, and locations further supports the idea that it has learned robust spatial priors, enabling generalization across a heterogeneous population.

These findings suggest that internal organ anatomy can be successfully estimated directly from body surface depth information, highlighting its value as a non-invasive surrogate for internal imaging. This demonstrates the potential of integrating camera-based organ localization into radio-

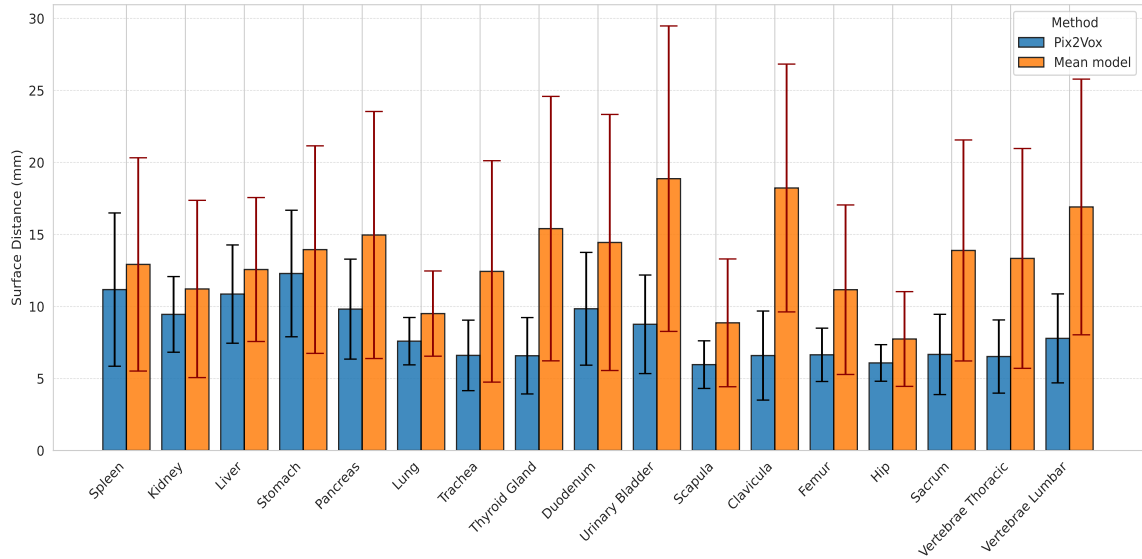


Figure 5: Average Symmetric Surface Distance (ASSD) for volumetric organs segmentation. Values are averaged for bilateral organs (e.g., kidneys, lungs) and vertebral subgroups (thoracic and lumbar vertebrae). Pix2Vox exhibits markedly lower surface distances compared to the mean model, indicating superior boundary accuracy and shape fidelity.

logical workflows, where such technology could enhance scan planning and optimize patient positioning.

## 5. Discussion

In this study, we introduce an approach for automated patient positioning that leverages body surface depth images to estimate the 3D position and shape of internal organs. Our quantitative and qualitative results demonstrate the feasibility of using a single depth image to approximate the internal anatomical layout. The proposed Pix2Vox model successfully learns to extract cues from surface morphology, such as torso shape, curvature, and contour depth, to predict the volumetric extent and spatial orientation of internal organs.

The model’s strong localization accuracy across multiple organs a promising direction to support scan planning and optimize table positioning without the need for external markers or scout imaging. Automated positioning could reduce reliance on trial-and-error adjustments by radiology technicians, potentially decreasing scan time, improving reproducibility, and reducing inter-operator variability. Additionally, the model’s capacity to generalize across diverse patient anatomies, as evidenced by its performance on a large and heterogeneous test set, underlines its robustness in dealing with physiological variation.

Despite these encouraging findings, several limitations and opportunities for future research must be acknowledged:

- Domain gap between synthetic and real-world depth data: The depth images used in this study were synthetically generated from MRI-derived segmentations and surface

reconstructions, which may not fully capture the variability present in real-world depth camera outputs. In clinical environments, additional sources of noise, such as occlusions, limited spatial resolution, lighting artifacts, and sensor-specific distortions, can affect image quality. Furthermore, patients may be covered with blankets, wear hospital gowns, or use assistive devices, all of which can obscure key body surface features. Bridging this domain gap is crucial for real-world applicability and may require domain adaptation techniques or model fine-tuning using real sensor-acquired data.

- Assumption of consistent patient pose and orientation: The training data used in this work consisted of patients in a standardized supine position with minimal variation in posture. Although position-based data augmentations were employed during training to increase robustness, real-world scenarios often involve a wider range of patient poses due to comfort needs or mobility restrictions. The current model may be sensitive to these variations, and further research is needed to evaluate and improve its generalizability to diverse body orientations and clinical settings.

## Acknowledgments

We gratefully acknowledge the financial support by German Research Foundation: DFG, HE 7364/10-1, project number 500498869.

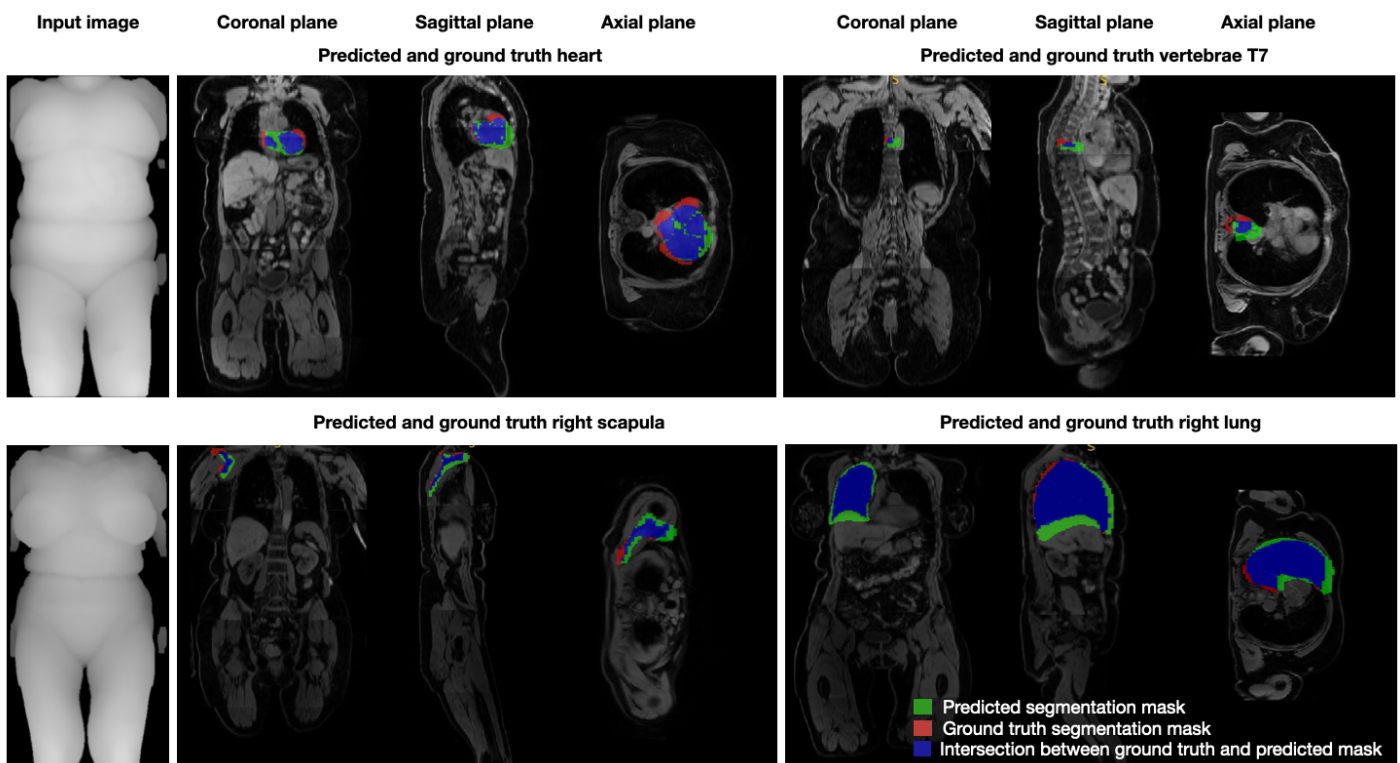


Figure 6: Qualitative comparison between predicted and ground truth volumetric segmentations. The Pix2Vox model demonstrates a strong ability to accurately infer both the shape and location of internal organs solely from a single depth image. The examples highlight successful predictions for both bony (vertebrae and scapula) and soft tissue organs (lung and heart) across different organ sizes and positions.

## Ethical Standards

The work follows appropriate ethical standards in conducting research and writing the manuscript, following all applicable laws and regulations regarding treatment of animals or human subjects.

## Conflicts of Interest

We declare we do not have conflicts of interest.

## Data availability

Data from the German National Cohort (NAKO) are available for research purposes upon registration and formal request through the NAKO Research Platform: <https://nako.de/en/research/>. Access is subject to approval by the NAKO Data Use and Access Committee and compliance with data protection regulations.

## References

F Bamberg. Whole-body magnetic resonance imaging in the german national cohort (nako): Design & current status. *European Journal of Public Health*, 32 (Supplement\_3):ckac129–029, 2022.

Ronald Booij, Ricardo PJ Budde, Marcel L Dijkshoorn, and Marcel van Straten. Accuracy of automated patient positioning in ct using a 3d camera for body contour detection. *European Radiology*, 29(4):2079–2088, 2019.

Ronald Booij, Marcel van Straten, Andreas Wimmer, and Ricardo PJ Budde. Automated patient positioning in ct using a 3d camera for body contour detection: accuracy in pediatric patients. *European radiology*, 31 (1):131–138, 2021.

Mikhail G Danilouchkine, Jos JM Westenberg, Albert de Roos, Johan HC Reiber, and Boudeijn PF Lelieveldt. Operator induced variability in cardiovascular mr: left ventricular measurements and their reproducibility. *Journal of Cardiovascular Magnetic Resonance*, 7(2):447–457, 2005.

Tugba Akinci D'Antonoli, Lucas K Berger, Ashraya K Indrakanti, Nathan Vishwanathan, Jakob Weiß, Matthias

Jung, Zeynep Berkarda, Alexander Rau, Marco Reisert, Thomas Küstner, et al. Totalsegmentator mri: Sequence-independent segmentation of 59 anatomical structures in mr images. *arXiv preprint arXiv:2405.19492*, 2024.

Kai Geißler, Daniel Mensing, Temke Kohlbrandt, Jochen G Hirsch, and Stefan Heldmann. Predicting anatomical structures from 2d depth images of patients. In *Medical Imaging 2025: Image Processing*, volume 13406, pages 407–411. SPIE, 2025.

Robert Graf, Paul-Sören Platzek, Evamaria Olga Riedel, Constanze Ramschütz, Sophie Starck, Hendrik Kristian Möller, Matan Atad, Henry Völzke, Robin Bülow, Carsten Oliver Schmidt, et al. Totalvibesegmentator: Full body mri segmentation for the nako and uk biobank. *arXiv preprint arXiv:2406.00125*, 2024.

Hengtao Guo, Benjamin Planche, Meng Zheng, Srikrishna Karanam, Terrence Chen, and Ziyan Wu. Smpl-a: Modeling person-specific deformable anatomy. In *Proceedings of the IEEE/CVF Conference on Computer Vision and Pattern Recognition*, pages 20814–20823, 2022.

H Häntze, L Xu, FJ Dorfner, et al. Mrsegmentator: robust multi-modality segmentation of 40 classes in mri and ct sequences. arxiv 2405.06463 [preprint] <https://arxiv.org/abs/2405.06463>. posted may 10, 2024. updated november 14, 2024. Accessed October, 2, 2024.

Reinhard Heckel, Mathews Jacob, Akshay Chaudhari, Or Perlman, and Efrat Shimron. Deep learning for accelerated and robust mri reconstruction. *Magnetic Resonance Materials in Physics, Biology and Medicine*, 37(3):335–368, 2024.

Pit Henrich and Franziska Mathis-Ullrich. Looc: Localizing organs using occupancy networks and body surface depth images. *IEEE Access*, 2025.

Kağan İncetan, Rishi Mohan, Henry Stoutjesdijk, Nelson Fernandes, and Bram de Jager. Rgb-d camera-based clinical workflow optimization for rotational angiography. *IEEE Sensors Journal*, 20(15):8867–8874, 2020.

Alexander Jaus, Constantin Seibold, Kelsey Hermann, Alexandra Walter, Kristina Giske, Johannes Haubold, Jens Kleesiek, and Rainer Stiefelhagen. Towards unifying anatomy segmentation: automated generation of a full-body ct dataset via knowledge aggregation and anatomical guidelines. *arXiv preprint arXiv:2307.13375*, 2023.

Srikrishna Karanam, Ren Li, Fan Yang, Wei Hu, Terrence Chen, and Ziyan Wu. Towards contactless patient positioning. *IEEE transactions on medical imaging*, 39(8):2701–2710, 2020.

Eytan Kats, Kai Geißler, Jochen G Hirsch, Stefan Heldmann, and Mattias P Heinrich. Internal organ localization using depth images: A framework for automated mri patient positioning. In *BVM Workshop*, pages 324–329. Springer, 2025.

Marilyn Keller, Silvia Zuffi, Michael J Black, and Sergi Pujades. Osso: Obtaining skeletal shape from outside. In *Proceedings of the IEEE/CVF conference on computer vision and pattern recognition*, pages 20492–20501, 2022.

Marilyn Keller, Vaibhav Arora, Abdelmouttaeb Dakri, Shivam Chandhok, Jürgen Machann, Andreas Fritzsche, Michael J Black, and Sergi Pujades. Hit: Estimating internal human implicit tissues from the body surface. In *Proceedings of the IEEE/CVF Conference on Computer Vision and Pattern Recognition*, pages 3480–3490, 2024.

Peter Koken, Sebastian PM Dries, Jochen Keupp, Daniel Bystrov, Vladimir Pekar, and Peter Börnert. Towards automatic patient positioning and scan planning using continuously moving table mr imaging. *Magnetic Resonance in Medicine: An Official Journal of the International Society for Magnetic Resonance in Medicine*, 62(4):1067–1072, 2009.

Matthew Loper, Naureen Mahmood, Javier Romero, Gerard Pons-Moll, and Michael J Black. Smpl: a skinned multi-person linear model. *ACM Transactions on Graphics (TOG)*, 34(6):1–16, 2015.

Daniel Mensing, Kai Geißler, Jochen Hirsch, Stefan Heldmann, and Matthias Günther. Mr-to-ct synthesis for cross-modality model adaptation. In *Medical Imaging 2025: Image Processing*, volume 13406, pages 447–455. SPIE, 2025.

Banafshe Shafieizargar, Riwaj Byanju, Jan Sijbers, Stefan Klein, Arnold J den Dekker, and Dirk HJ Poot. Systematic review of reconstruction techniques for accelerated quantitative mri. *Magnetic Resonance in Medicine*, 90(3):1172–1208, 2023.

Karthik Shetty, Annette Birkhold, Srikrishna Jaganathan, Norbert Strobel, Bernhard Egger, Markus Kowarschik, and Andreas Maier. Boss: Bones, organs and skin shape model. *Computers in Biology and Medicine*, 165:107383, 2023.

Brian Teixeira, Vivek Singh, Birgi Tamersoy, Andreas Prokein, and Ankur Kapoor. Automated ct lung cancer screening workflow using 3d camera. In *International Conference on Medical Image Computing and Computer-Assisted Intervention*, pages 423–431. Springer, 2023.

Marthinus B Van Rooyen and Richard D Pitcher. The cinderellas of the scanner: Magnetic resonance imaging'pre-scan'and'post-scan'times: Their determinants and impact on patient throughput. *SA Journal of Radiology*, 24(1):1–6, 2020.

Jakob Wasserthal, Hanns-Christian Breit, Manfred T Meyer, Maurice Pradella, Daniel Hinck, Alexander W Sauter, Tobias Heye, Daniel T Boll, Joshy Cyriac, Shan Yang, et al. Totalsegmentator: robust segmentation of 104 anatomic structures in ct images. *Radiology: Artificial Intelligence*, 5(5):e230024, 2023.

Yifan Wu, Vivek Singh, Brian Teixeira, Kai Ma, Birgi Tamersoy, Andreas Krauss, and Terrence Chen. Towards generating personalized volumetric phantom from patient's surface geometry. In *Medical Image Computing and Computer Assisted Intervention—MICCAI 2018: 21st International Conference, Granada, Spain, September 16–20, 2018, Proceedings, Part I*, pages 171–179. Springer, 2018.